KYBERNETIKA — VOLUME *54* (2018), NUMBER 5, PAGES 978–990

REGION OF INTEREST CONTRAST MEASURES

Václav Remeš and Michal Haindl

A survey of local image contrast measures is presented and a new contrast measure for measuring the local contrast of regions of interest is proposed. The measures validation is based on the gradual objective contrast decreasing on medical test images in both grayscale and color. The performance of the eleven most frequented contrast measures is mutually compared and their robustness to different types of image degradation is analyzed. Since the contrast measures can be both global, regional and local pixelwise, a simple way of adapting the contrast measures for regions of interest is proposed.

Keywords: contrast measures, image enhancement, enhancement quality measures, medical image enhancement

Classification: 68U10, 94A08

1. INTRODUCTION

Image enhancement methods aim to improve human image interpretation accuracy by increasing visual distinguishability of single objects recorded in a visual scene. This requires an increase in image contrast which is the relative difference in luminance or colour between multiple objects.

Typical important image enhancement applications are in selected medical areas through computer aided diagnosis, remote sensing, and various security videos interpretation. Among the most important are the medical applications. Not only because they have the potential to save human lives, but also because medical doctors rarely rely on fully automatic image analysis systems and generally prefer visual reading of data.

Numerous image enhancement methods have been published for preventive mammography screening [3, 5, 6, 8, 12, 15, 18, 19, 22, 24, 26, 29]. Around 25% of radiologically visible cancers are missed by the radiologists at screening [23] which means that millions of cancer cases are missed every year. This directly impacts the mortality rate for women, because breast cancer is the most common type of cancer among middle-aged women in most developed countries [17, 25] and almost one woman in ten grows a breast cancer in her life. In such important image enhancement applications even a slightest improvement in the detection methods could have a huge impact and save many lives.

A reliable quality contrast measure is then the prerequisite for any monitoring of an image enhancement method development progress or for ranking existing methods.

DOI: 10.14736/kyb-2018-5-0978

The paper is organized as follows: Section 2 presents an overview of existing contrast measures, in Section 3 we describe our proposed contrast measure and Section 4 covers the extensive comparison of previously published criteria with our own method. The paper is summarized in Section 5.

2. CONTRAST MEASURES

The contrast measure is not uniquely defined [16, 20] and many measures, which are usually categorized into local and global measures, are available. Another possible categorization is whether they use only monospectral information, e. g., the Weber contrast(WC), Michelson contrast (MC), root-mean-square contrast (RMS), measure of enhancement (EME), enhancement by entropy (EMEE), Michelson law measure of enhancement (AME), Michelson law measure of enhancement by entropy (AMEE), second-derivative-like enhancement measure (SDME), difference-of-Gaussians based contrast measures (C1, C2, C3, (1) – (13)), local band-limited contrast (LBLC), region contrast (RCC, (18)), or they use all three colour bands, e. g., the weighted-level framework with retinal-like sub-sampling contrast (Wlf_{Rsc} (15)), border contrast (BCC (19)). Typical measures used are the Weber or Michelson contrast measures. The Weber contrast [27] is

$$\uparrow WC = \frac{Y_{obj} - Y_{back}}{Y_{back}} \qquad \geq -1 \ , \qquad (1)$$

where $\uparrow$ is the required measure movement, Y_{obj}, Y_{back} are the object and background luminance, respectively. The Michelson contrast [13] is defined as

$$\uparrow MC = \frac{Y_{\max} - Y_{\min}}{Y_{\max} + Y_{\min}} \qquad \geq 0 \ , \qquad (2)$$

where $Y_{\max}, Y_{\min}$ are the highest and lowest luminances. The Michelson contrast measure is not appropriate for images with extremal isolated bright or dark pixels which will create a discrepancy between the measure value and the perceived contrast. If we can set $Y_{obj} = Y_{\max}$ and $Y_{back} = Y_{\min}$ then both measures are related:

$$MC = WC \, \frac{Y_{back}}{Y_{obj} + Y_{back}} \ .$$

Several modifications [4, 10, 28] of this measure which replace either $Y_{\max}$ or $Y_{\min}$ with Y_{mean} were also published.

2.1. Global contrast measures

A simple used global contrast crierion is the root-mean-square contrast

$$\uparrow RMS = \left[\frac{1}{n_1 n_2 - 1} \sum_{r_1=1}^{n_1} \sum_{r_2=1}^{n_2} (\hat{Y}_{r_1,r_2} - \mu)^2 \right]^{\frac{1}{2}} \ , \qquad (3)$$

where $n_1 \times n_2$ is image resolution, $\hat{Y}$ is a normalized gray-level image such that $\hat{Y}_{r_1,r_2} \in [0;1]$ $\forall r_1, r_2$, and μ is the mean normalized gray level. This measure does not depend on the spatial distribution of contrast in the image.

The measure of enhancement (EME) based on a Weber-law-based contrast measure was proposed by Agaian [1] and analogically the measure of enhancement by entropy (EMEE). The Michelson law measure of enhancement (AME) and its entropy modification, Michelson law measure of enhancement by entropy (AMEE), were later proposed by the same authors [2]. Panetta et al. [15] used these global monospectral contrast measures for mammogram enhancement assessment and introduced a second-derivative-like enhancement measure (SDME). The SDME results were found to be consistent with the mean opinion score (MOS) from seven human observers, while the AME, AMEE, EME, EMEE measures were found to be inconsistent [15]. All these contrast measures assume an evaluated image divided into $k_1 \times k_2$ blocks.

$$\uparrow EME_{k_1,k_2} = \frac{1}{k_1\, k_2} \sum_{l=1}^{k_1} \sum_{k=1}^{k_2} 20 \ln \left(\frac{Y_{\max,k,l}}{Y_{\min,k,l}} \right) \qquad \langle 0; \infty) \ , \quad (4)$$

$$\uparrow EMEE_{k_1,k_2} = \frac{1}{k_1\, k_2} \sum_{l=1}^{k_1} \sum_{k=1}^{k_2} \left[\alpha \left(\frac{Y_{\max,k,l}}{Y_{\min,k,l}} \right)^{\alpha} \ln \left(\frac{Y_{\max,k,l}}{Y_{\min,k,l}} \right) \right] \qquad \langle 0; \infty) \ , \quad (5)$$

$$\downarrow AME_{k_1,k_2} = -\frac{1}{k_1\, k_2} \sum_{l=1}^{k_1} \sum_{k=1}^{k_2} 20 \ln \left(\frac{Y_{\max,k,l} - Y_{\min,k,l}}{Y_{\max,k,l} + Y_{\min,k,l}} \right) \qquad \langle 0; \infty) \ , \quad (6)$$

$$\downarrow AMEE_{k_1,k_2} = \frac{-\alpha}{k_1\, k_2} \sum_{l=1}^{k_1} \sum_{k=1}^{k_2} \left(\frac{Y_{\max,k,l} - Y_{\min,k,l}}{Y_{\max,k,l} + Y_{\min,k,l}} \right)^{\alpha} \ln \left(\frac{Y_{\max,k,l} - Y_{\min,k,l}}{Y_{\max,k,l} + Y_{\min,k,l}} \right) \qquad \langle 0; \infty) \ , \quad (7)$$

$$\downarrow SDME_{k_1,k_2} = -\frac{1}{k_1\, k_2} \sum_{l=1}^{k_1} \sum_{k=1}^{k_2} 20 \ln \left(\frac{Y_{max,k,l} - 2Y_{center,k,l} + Y_{\min,k,l}}{Y_{\max,k,l} + 2Y_{center,k,l} + Y_{\min,k,l}} \right) \qquad \langle 0; \infty) \ , \quad (8)$$

where α is a constant, $Y_{\max,k,l}, Y_{\min,k,l}, Y_{center,k,l}$ are the corresponding maximum, minimum, and center values, respectively.

The main disadvantage of these global measures is their insufficient robustness. They exhibit strong dependence on two single extreme brightness or darkness points (possibly outliers), while the overall contrast perception might be completely different.

2.2. Local pixelwise contrast measures

2.2.1. Difference-of-Gaussians based contrast measures

Three different local contrast measures ($C1, C2, C3$) based on the difference of Gaussians were introduced by Tadmor and Tolhurst [21]. These contrast measures (especially $C3$) should model the response of the eye to the variations in contrast.

$$Cen(i,j) = exp\left[-\left(\frac{i}{\rho_c} \right)^2 - \left(\frac{j}{\rho_c} \right)^2 \right] \ ,$$

$$Sur(i,j) = 0.85 \left(\frac{\rho_c}{\rho_s} \right)^2 exp\left[-\left(\frac{i}{\rho_s} \right)^2 - \left(\frac{j}{\rho_s} \right)^2 \right] \ ,$$

$$R_c(x,y) = \sum_{i=x-3\rho_c}^{x+3\rho_c} \sum_{j=y-3\rho_c}^{y+3\rho_c} Cen(i-x, j-y) Y_{i,j} \ , \tag{9}$$

$$R_s(x,y) = \sum_{i=x-3\rho_s}^{x+3\rho_s} \sum_{j=y-3\rho_s}^{y+3\rho_s} Sur(i-x, j-y) Y_{i,j} \ , \tag{10}$$

$$\uparrow C1(x,y) = \frac{R_c(x,y) - R_s(x,y)}{R_c(x,y)} \ , \tag{11}$$

$$\uparrow C2(x,y) = \frac{R_c(x,y) - R_s(x,y)}{R_s(x,y)} \ , \tag{12}$$

$$\uparrow C3(x,y) = \frac{R_c(x,y) - R_s(x,y)}{R_c(x,y) + R_s(x,y)} \ , \tag{13}$$

where ρ_c and ρ_s denote the radius for the centered and surrounding Gaussian respectively, $\rho_c < \rho_s$, and x, y are spatial indices.

2.2.2. Weighted-level framework

The Weighted-Level Framework with Retinal-like sub-sampling contrast, Wlf_{Rsc} method [20], works in the CIELAB (or RGB) color space averaging the values of the actual bands. It is based on the idea of the normalized difference of Gaussians used in the C3 criterion 13 combined with the Gaussian pyramid

$$Wlf_{Rsc,i} = \frac{1}{N_l} \sum_{l=1}^{N_l} \lambda_l E_l\{C3_i\} \ , \tag{14}$$

$$\uparrow Wlf_{Rsc} = \sum_{k=1}^{d} c_i Wlf_{Rsc,i} > 0 \ , \tag{15}$$

where N_l is the number of levels in the Gaussian pyramid, $E_l\{...\}$ is the mean value of the given contrast measure at the sub-sampled level l, d is the number of spectral bands, λ_l is the weight of level l and $C3_i$ is from (13) computed on the ith spectral channel, and c_i are the weights of each color channel. For the RGB color space Simone et al.[20] suggest c_i to be the variance of pixel values for the corresponding channel, while in the Lab color space they propose to use $c_i = 0.33 \ \forall i$.

2.2.3. Local band-limited contrast

The Local band-limited contrast [9, 16] uses an approach based on the Fourier transform. To define the local ith band-limited contrast, the frequency band-limited version of the image is first obtained in the frequency domain $A_i(u,v)$ by using a radially symmetric band-pass filter $G_i(r)$

$$A_i(u,v) \equiv A_i(r,\theta) = F(r,\theta) G_i(r) \ ,$$

where $F(r,\theta)$ is the Fourier transform of the original image in polar coordinates r,θ. The ith band filter G_i can be expressed as

$$G_i(r) = \begin{cases} \frac{1}{2}\left[1 + cos(\pi \log_2 r - \pi i)\right], & \text{if } r \in \left\langle 2^i; 2^{i+1}\right) \\ 0, & \text{otherwise.} \end{cases}$$

The original image can be expressed as the sum of local band-filtered images (a_i being the inverse Fourier transforms of A_i) and a low pass and high pass residuum (l_0 and h_n respectively, n is the selected number of frequency bands) in the following equation:

$$f(x,y) = l_0(x,y) + \sum_{i=1}^{n-1} a_i(x,y) + h_n(x,y) \ .$$

For every pixel, the contrast in frequency band i can be computed as

$$c_i(x,y) = \frac{a_i(x,y)}{l_0(x,y) + \sum_{j=1}^{i-1} a_j(x,y)} \ .$$

For expressing the contrast in each pixel, we took the sum of absolute values of the local contrasts

$$LBLC(x,y) = \sum_{i=1}^{n} |c_i(x,y)| \ , \tag{16}$$

because the authors have only specified the contrast up to the frequency bands, omitting the final merging of the contrast information.

2.3. Region of interest based contrast measures

2.3.1. Region contrast

The contrast between two regions is computed on the basis of the average values of features of adjacent regions [11]:

$$\begin{aligned} c_{i,j} &= \frac{|\mu_i - \mu_j|}{\mu_i + \mu_j} \\ k_{i,j} &= \frac{|border(i) \bigcap border(j)|}{|border(i)|} \\ c_i &= \sum_{\forall R_j adj\ R_i} k_{i,j} c_{i,j} \qquad (17) \\ \uparrow RCC &= \frac{\sum_{\forall Rj} |R_j| c_j}{\sum_{\forall Rj} |R_j|} > 0 \qquad (18) \end{aligned}$$

where μ_i denotes the mean value of region i, $border(i)$ are the pixels on the border of region i, and $adjR_i$ are regions which are adjacent to region i. Equation (17) computes the contrast of ith region and equation (18) sums the global contrast.

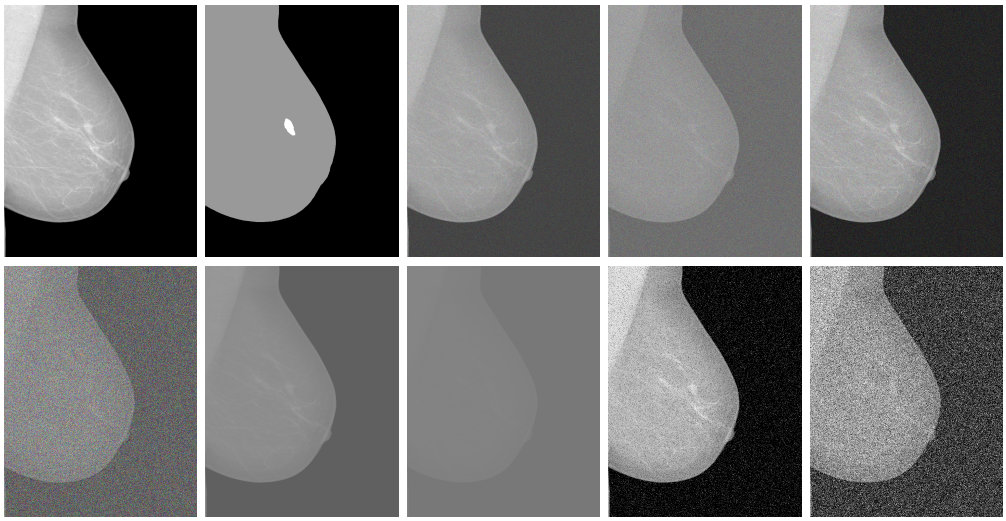

Fig. 1. Experimental mammogram, its region of interest template, and its corruption using the additive Gaussian noise $\sigma = 30, \sigma = 100$, additive noise with uniform noise 30% blending (upper row left to right). Additive noise with uniform noise 80%, range reduction 2 bits, range reduction 4 bits, salt and pepper noise 10%, and 50%, respectively (lower row).

2.3.2. Border contrast

The contrast measure [7] computes the mean difference of pixel values along the border of a region of interest. For each region of interest R_i and all border pixels $b(R_i)$ it computes the mean pixel values μ_{in_j} and μ_{out_j} of small windows next to the border inside and outside of the desired region of interest, normalized by the image's maximum pixel value $Y_{\max}$. The value of n_s is a normalization factor denoting the number of spectral bands of the image so that gray-scale images can be compared with multispectral ones.

$$\uparrow BCC = \frac{100}{Y_{\max}\sqrt{n_s}} \sum_i |b(R_i)| \sum_i \sum_{j \in b(R_i)} ||\mu_{in_j} - \mu_{out_j}|| > 0 \ . \tag{19}$$

3. PROPOSED REGION OF INTEREST CONTRAST MEASURES

3.1. Multispectral region of interest contrast measure

We propose a simple multispectral contrast measure (SRC) loosely based on the Region contrast (18) [11]. The main idea is that the distinguishability of a region is mostly influenced by its direct surroundings. Let's define the surroundings $S_{i,d}$ of region i as all pixels which do not belong to the region i and their distance from the region in both

x and y axes is at most d. The surrounding region contrast

$$SRC = \frac{||\mu_i - \mu_{S_{i,d}}||}{||\mu_i + \mu_{S_{i,d}}||} \ , \tag{20}$$

where μ_i is the mean spectral vector of the ith region and $\mu_{S_{i,d}}$ is the mean spectral vector of its surroundings up to the distance d.

The distance d of the surroundings can be determined as either a constant value or relative to the size of the region of interest.

3.2. Modifying contrast measures for regions of interest

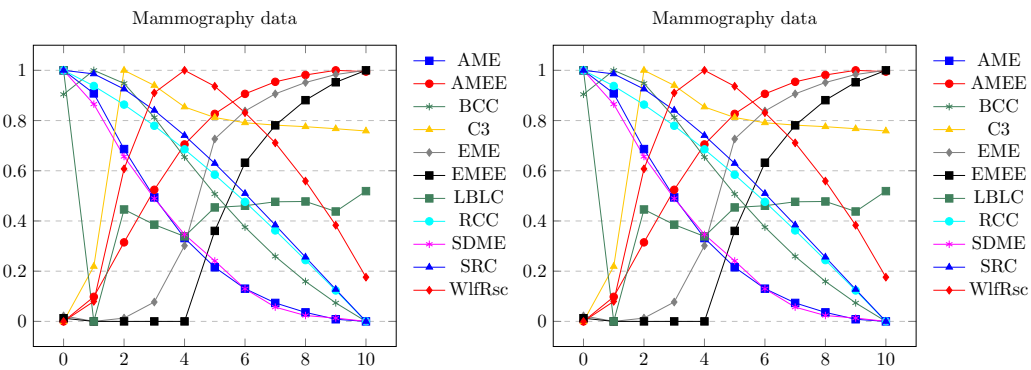

Fig. 2. The measures behaviour for the averaging image degradation. Left: dermatological data (colour), right: mammography data (grayscale).

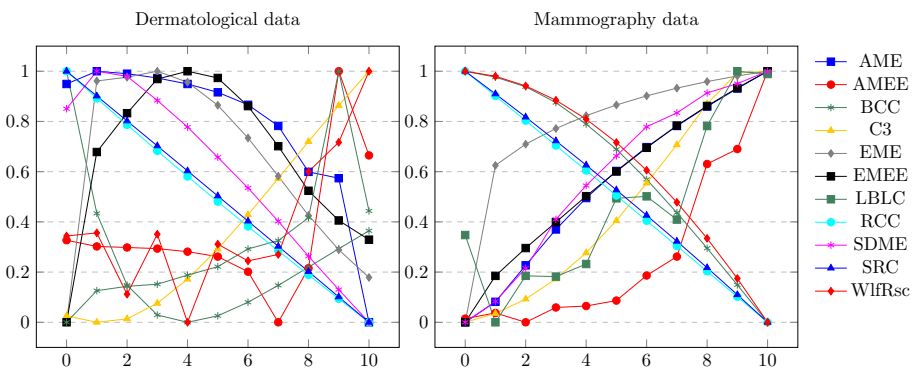

Fig. 3. The measures behaviour for the Gaussian noise image degradation. Left: dermatological data (colour), right: mammography data (grayscale).

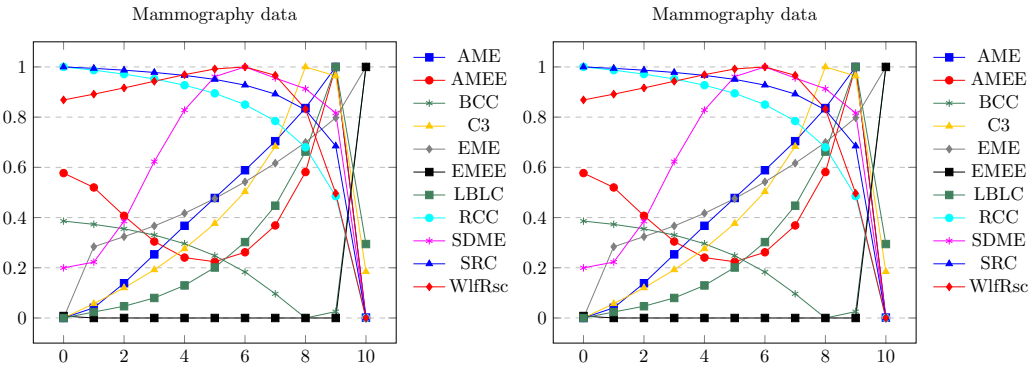

Fig. 4. The measures behaviour for the uniform noise image degradation. Left: dermatological data (colour), right: mammography data (grayscale).

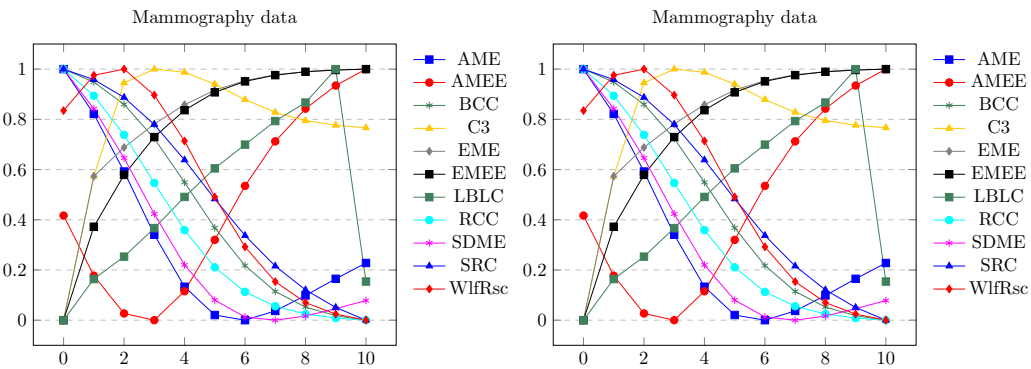

Fig. 5. The measures behaviour for the range reduction image degradation. Left: dermatological data (colour), right: mammography data (grayscale).

Measuring the contrast for local abnormality enhancement is somewhat dubious since ideally we want to lower the contrast of normal texture as much as possible and only raise the contrast of the abnormalities. Denoting an object O and B as background, we propose the following modification to contrast measures to make them suitable for measuring the contrast of regions of interest:

$$ContrastFactor = \frac{Contrast(O)}{Contrast(B \setminus O)} \ , \tag{21}$$

where $Contrast(\cdot)$ is an arbitrary global contrast measure.

This way we can compute the factor by which the contrast at the abnormality is

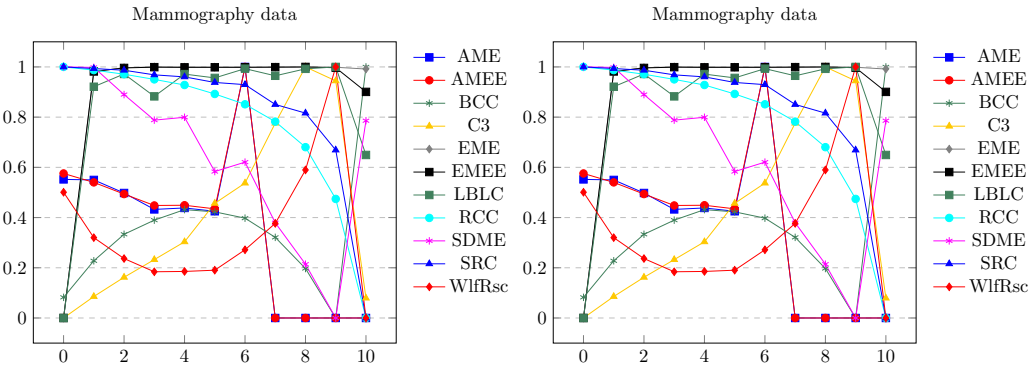

Fig. 6. The measures behaviour for the salt and pepper noise image degradation. Left: dermatological data (colour), right: mammography data (grayscale).

greater (or lower) than the contrast in the rest of the breast image. The same equation can be directly applied to all the global contrast measures such as the SDME (8). For local contrast measures, which give local contrast values for each pixel (denoted $L(x, y)$, where x, y are spatial indices), such as the Wlf_{Rsc} (15), we sum the values for each pixel beforehand and take their mean value:

$$ContrastFactor = \frac{|B \setminus O|}{|O|} \frac{\sum_{x,y \in O} L(x, y)}{\sum_{x,y \in (B \setminus O)} L(x, y)}. \tag{22}$$

3.3. Multispectral generalization of the grayscale contrast measures

The straightforward generalization of monospectral contrast measures $C(.\ )$ to any d number of spectral bands is

$$C_Q = [C_1, \ldots, C_d]\, Q\, [C_1, \ldots, C_d]^T \ , \tag{23}$$

where Q is some appropriate positive definite weighting matrix. Q can be the unity matrix $Q = diag[1, \ldots, 1]$ or for color images it can be their grayscale conversion, e. g., converted from the RGB color space:

$$Q = \begin{pmatrix} 0.2989 & 0 & 0 \\ 0 & 0.587 & 0 \\ 0 & 0 & 0.114 \end{pmatrix} .$$

Other possibilities, e. g. those proposed by Simone et al. [20], include using the variance of each channel's values as the weight or $\frac{1}{\mu}$ where μ is the mean value in the colour channel.

	Dermatological data (colour)					Mammography data (grayscale)				
	AVG	GN	U	LC	SP	AVG	GN	U	LC	SP
AME	x	x	x	↑	x	↓	↑	↑	x	x
AMEE	↑	x	x	↑	x	x	x	x	x	x
BCC	↓	x	x	↓	↑	x	↓	x	↓	x
C3	x	↑	x	↑	x	x	↑	x	x	x
EME	x	x	x	x	x	x	↑	↑	↑	x
EMEE	x	x	x	x	x	x	↑	x	↑	x
LBLC	x	x	x	x	x	x	x	x	x	x
RCC	x	↓	↓	↓	↓	↓	↓	↓	↓	↓
SDME	x	x	↑	↑	x	↓	↑	x	x	x
SRC	↓	↓	↓	↓	↓	↓	↓	↓	↓	↓
Wlf_{Rsc}	↑	x	↑	↑	x	x	↓	x	x	x

Tab. 1. Summary of the behaviour of the different contrast measures among different degradations. ↑ means monotonous increasing, ↓ means monotonous decreasing and x means non-monotonous behaviour.

4. RESULTS

We have validated the contrast measures on the more than 100 grayscale images from the INbreast database [14] which include an abnormal mass and on 20 color skin images with cancer-like abnormalities using five different contrast degradation approaches (see Figure 1):

1. Additive Gaussian noise (**GN**), varying standard deviations ($\sigma \in \{10, 20, \ldots, 100\}$),
2. Salt and pepper noise (**SP**), varying ratio of presence ($10\%, 20\%, \ldots, 100\%$),
3. Linearly combined uniform noise (**U**) (0-255), ratio ($10\%, 20\%, \ldots, 100\%$),
4. Gray level range reduction (**LC**) ($\frac{1}{2}, \frac{1}{4}, \ldots, \frac{1}{1024}$),
5. Averaging (**AVG**) of values within windows of sizes $(1, 3, 5, \ldots, 21)$.

We illustrate our results in this article on INbreast data and on dermatological data, however, we obtained similar results using several other types of gray-scale or colour images.

The experiments use the parameters $k_1 = width/5, k_2 = height/5, \alpha = 0.5$ for AME, AMEE, EME, EMEE, SDME, for C3 and Wlf_{Rsc} (14) $\rho_c = 1, \rho_s = 2, N_l = 5, \lambda_l$ is the variance of pixel values in each channel at level l. For the BCC we have selected a window of size 3×3, with the window's center 5 pixels distant from the border. Since the C1 (11) and C2 (12) measures give values similar to C3 (correlation > 0.99), they are not included in the presented results.

In our proposed method, we set the parameter $d = 6$ to match the similarly parametrized compared contrast measures.

For a correctly functioning contrast measure, the corresponding degradation graph should be monotonous and consistent among the different image degradations. The results (plotted in the graphs in Figs. 2-6) demonstrate that the different contrast measures are not consistently reliable. The sole two exceptions are the Region contrast measure (18) which only fails in one case (averaging on the dermatological data), and our proposed Surrounding region contrast (20), which shows consistent results in all the experiments.

The presented graphs are normalized to the range $< 0; 1 >$ to provide better visual comparison. The horizontal axes start at 0 with the original images and the deterioration then increase rightwards.

Tab. 1 shows a summary of the behaviour of the different contrast measures. We can see that except for the SRC (20) measure, all the contrast measures exhibit non-monotony and the AME, BCC, SDME and Wlf_{Rsc} even show inconsistent monotonous behaviour (for some degradations, they are monotonously increasing while for others they are decreasing) with LBLC being inconsistent in all the cases. The second best enhancement measure is the RCC which only exhibited one minor non-monotony in one case but otherwise behaved consistently.

5. CONCLUSION

We have implemented a new contrast measure and compared it with ten different existing contrast measures. The contrast measures were tested on five gradual image degradation scenarios on both grayscale and colour medical images. It has been shown that for the purposes of region of interest enhancement validation, very few contrast measures can be trusted. The only contrast measures which are robust to different types of noise and range deterioration tested are the proposed Surrounding region contrast and the Region contrast measures. All the remaining measures failed in multiple tests and cannot be used for trustworthy development of region of interest enhancement methods. Needless to say, the results show only the usefulness of the contrast measures for automatic region of interest contrast validation. The measures themselves can be useful for alternative applications.

(Received February 2, 2018)

REFERENCES

[1] S. S. Agaian, K. Panetta, and A. M. Grigoryan: Transform-based image enhancement algorithms with performance measure. IEEE Trans. Image Process. *10* (2001), 3, 367–382. DOI:10.1109/83.908502

[2] S. S. Agaian, B. Silver, and K. A. Panetta: Transform coefficient histogram-based image enhancement algorithms using contrast entropy. IEEE Trans. Image Process. *16* (2007), 3, 741–758. DOI:10.1109/tip.2006.888338

[3] V. Bhateja, M. Misra, and S. Urooj: Non-linear polynomial filters for edge enhancement of mammogram lesions. Comp. Meth. Programs Biomedicine *129* (2016), 125–134. DOI:10.1016/j.cmpb.2016.01.007

[4] D. A. Burkhardt, J. Gottesman, D. Kersten, and G. E. Legge: Symmetry and constancy in the perception of negative and positive luminance contrast. JOSA A *1* (1984), 3, 309–316. DOI:10.1364/josaa.1.000309

[5] C.-M. Chang and A. Laine: Coherence of multiscale features for enhancement of digital mammograms. IEEE Trans. Inform. Technol. Biomedicine *3* (1999), 1, 32–46. DOI:10.1109/4233.748974

[6] S. Dippel, M. Stahl, R. Wiemker, and T. Blaffert: Multiscale contrast enhancement for radiographies: Laplacian pyramid versus fast wavelet transform. IEEE Trans. Medical Imaging *21* (2002), 4, 343–353. DOI:10.1109/tmi.2002.1000258

[7] C. E. Erdem, B. Sankur, and A. M. Tekalp: Performance measures for video object segmentation and tracking. IEEE Trans. Image Process. *13* (2004), 7, 937–951. DOI:10.1109/tip.2004.828427

[8] J. Grim, P. Somol, M. Haindl, and J. Daneš: Computer-aided evaluation of screening mammograms based on local texture models. IEEE Trans. Image Process. *18* (2009), 4, 765–773. DOI:10.1109/tip.2008.2011168

[9] A. Haun and E. Peli: Perceived contrast in complex images. J. Vision *13* (2013), 3, 2013. DOI:10.1167/13.13.3

[10] P. E. King-Smith and J. Kulikowski: Pattern and flicker detection analysed by subthreshold summation. J. Physiology *249* (1975), 3, 519. DOI:10.1113/jphysiol.1975.sp011028

[11] M. D. Levine and A. M. Nazif: Dynamic measurement of computer generated image segmentations. IEEE Trans. Pattern Analysis Machine Intell. *7* (1985), 155–164. DOI:10.1109/tpami.1985.4767640

[12] A. Mencattini, M. Salmeri, R. Lojacono, M. Frigerio, and F. Caselli: Mammographic images enhancement and denoising for breast cancer detection using dyadic wavelet processing. IEEE Trans Instrument. Measurement *57* (2008), 7, 1422–1430. DOI:10.1109/tim.2007.915470

[13] A. A. Michelson: Studies in Optics. University of Chicago Press, Chicago 1927.

[14] I. C. Moreira, I. Amaral, I. Domingues, A. Cardoso, M. J. Cardoso, and J. S. Cardoso: Inbreast: toward a full-field digital mammographic database. Academic Radiology *19* (2012), 2, 236–248. DOI:10.1016/j.acra.2011.09.014

[15] K. Panetta, Y. Zhou, S. Agaian, and H. Jia: Nonlinear unsharp masking for mammogram enhancement. IEEE Trans. Inform. Technol. Biomedicine *15* (2011), 6, 918–928. DOI:10.1109/titb.2011.2164259

[16] E. Peli: Contrast in complex images. JOSA A *7* (1990), 10, 2032–2040. DOI:10.1364/josaa.7.002032

[17] H. Qi and N. A. Diakides: Thermal infrared imaging in early breast cancer detection – a survey of recent research. In: Proc. 25th Annual International Conference of the IEEE Engineering in Medicine and Biology Society, Vol. 2, IEEE 2003, pp. 1109–1112. DOI:10.1109/iembs.2003.1279442

[18] P. Sakellaropoulos, L. Costaridou, and G. Panayiotakis: A wavelet-based spatially adaptive method for mammographic contrast enhancement. Physics Medicine Biology *48* (2003), 6, 787. DOI:10.1088/0031-9155/48/6/307

[19] J. Salvado and B. Roque: Detection of calcifications in digital mammograms using wavelet analysis and contrast enhancement. In: IEEE International Workshop on Intelligent Signal Processing 2005, IEEE 2005, pp. 200–205. DOI:10.1109/wisp.2005.1531658

[20] G. Simone, M. Pedersen, and J. Y. Hardeberg: Measuring perceptual contrast in digital images. J. Visual Commun. Image Representation *23* (2012), 3, 491–506. DOI:10.1016/j.jvcir.2012.01.008

[21] Y. Tadmor and D. Tolhurst: Calculating the contrasts that retinal ganglion cells and {LGN} neurones encounter in natural scenes. Vision Research *40* (2000), 22, 3145–3157. DOI:10.1016/s0042-6989(00)00166-8

[22] J. Tang, X. Liu, and Q. Sun: A direct image contrast enhancement algorithm in the wavelet domain for screening mammograms. IEEE J. Selected Topics Signal Process. *3* (2009), 1, 74–80. DOI:10.1109/jstsp.2008.2011108

[23] P. Taylor, J. Champness, R. Given-Wilson, K. Johnston, and H. Potts: Impact of computer-aided detection prompts on the sensitivity and specificity of screening mammography. Health Technol. Assessment *9* (2005), 6. DOI:10.3310/hta9060

[24] K. Thangavel, M. Karnan, R. Sivakumar, and A. Mohideen: Cad system for preprocessing and enhancement of digital mammograms. Graphics, Vision Image Process. *xx* (2007), 55–60.

[25] T. Tweed and S. Miguet: Automatic detection of regions of interest in mammographies based on a combined analysis of texture and histogram. In: Proc. 16th International Conference on Pattern Recognition 2002, Vol. 2, Los Alamitos 2002. IEEE Computer Soc., pp. 448–452. DOI:10.1109/icpr.2002.1048335

[26] H. Wang, J.-B. Li, L. Wu, and H. Gao: Mammography visual enhancement in cad-based breast cancer diagnosis. Clinical Imaging *37* (2013), 273–282. DOI:10.1016/j.clinimag.2012.04.018

[27] E. H. Weber: The Sense of Touch. Academic Press, 1978.

[28] P. Whittle: Increments and decrements: Luminance discrimination. Vision Res. *26* (1986), 10, 1677–1691. DOI:10.1016/0042-6989(86)90055-6

[29] Z. Yan, Y. Zhang, B. Liu, J. Zheng, L. Lu, Y. Xie, Z. Liang, and J. Li: Extracting hidden visual information from mammography images using conjugate image enhancement software. In: IEEE International Conference on Information Acquisition, IEEE Engineering in Medicine and Biology Society, 2005, pp. 4775–4778. DOI:10.1109/icia.2005.1635092

Václav Remeš, Institute of Information Theory and Automation, The Czech Academy of Sciences, Pod Vodárenskou věží 4, 182 08 Praha 8. Czech Republic.
e-mail: remes@utia.cz

Michal Haindl, Institute of Information Theory and Automation, The Czech Academy of Sciences, Pod Vodárenskou věží 4, 182 08 Praha 8. Czech Republic.
e-mail: haindl@utia.cz